Histol Histopathol (2016) 31: 189-204

http://www.hh.um.es

Histology and Histopathology

From Cell Biology to Tissue Engineering

MRL/MpJ mice show unique pathological features after experimental kidney injury

Daichi Shiozuru[1], Osamu Ichii[1], Junpei Kimura[1], Teppei Nakamura[1,2], Yaser Hosny Ali Elewa[1,3], Saori Otsuka-Kanazawa[1] and Yasuhiro Kon[1]

[1]Laboratory of Anatomy, Department of Biomedical Sciences, Graduate School of Veterinary Medicine, Hokkaido University, [2]Section of Biological Safety Research, Chitose Laboratory, Japan Food Research Laboratories, Chitose, Hokkaido, Japan and [3]Department of Histology and Cytology, Faculty of Veterinary Medicine, Zagazig University, Zagazig, Egypt

Summary. Clarification of the renal repair process is crucial for developing novel therapeutic strategies for kidney injury. MRL/MpJ mice have a unique repair process characterized by low scar formation. The pathological features of experimentally injured MRL/MpJ and C57BL/6 mouse kidneys were compared to examine the renal repair process.

The dilation and atrophy of renal tubules were observed in folic acid (FA)-induced acute kidney injury (AKI) in both strains, and the histopathological injury scores and number of interleukin (IL)-1F6-positive damaged distal tubules and kidney injury molecule 1 (KIM-1)-positive damaged proximal tubules drastically increased 1 day after AKI induction. However, KIM-1-positive tubules and the elevation of serum renal function markers were significantly fewer and lower, respectively, in MRL/MpJ mice at days 2 and 7 after AKI. After traumatic kidney injury (TKI) via needle puncture, severe tubular necrotic lesions in the punctured area and fibrosis progressed in both strains. Indices for fibrosis such as aniline blue-positive area, number of alpha smooth muscle actin-positive myofibroblasts, and messenger RNA expression levels of *Tgfb1* and *Mmp2* indicated lower fibrotic activity in MRL/MpJ kidneys. Characteristically, only MRL/MpJ kidneys manifested remarkable calcification around the punctured area beginning 7 days after TKI.

The pathological features of injured MRL/MpJ and C57BL/6 kidneys differed, especially those of kidneys with mild proximal tubular injuries after FA-induced AKI. Lower fibrotic activity and increased calcification after TKI were observed in MRL/MpJ kidneys. These findings clarified the unique pathological characteristics of MRL/MpJ mouse kidneys and contribute to understanding of the renal repair process after kidney injury.

Key words: Fibrosis, Kidney, MRL/MpJ mice, Repair

Offprint requests to: Yasuhiro Kon, Laboratory of Anatomy, Department of Biomedical Sciences, School of Veterinary Medicine, Hokkaido University, Kita 18-Nishi 9 Kita-ku, Sapporo, 060-0818, Japan. e-mail: y-kon@vetmed.hokudai.ac.jp

DOI: 10.14670/HH-11-662

Introduction

The pathological response to tissue injury can be divided into 2 main processes: regeneration and wound repair. Although the former, including the regeneration of cut limbs observed in amphibians, is unlikely to occur in mammals, the liver shows regenerative capabilities in several animals (Fausto, 2000). Wound repair is generally observed in injured tissues, and the proliferation, replenishment, or both of parenchymal cells contributes to the repair of injured organs such as skin (Naviaux et al., 2009), skeletal muscle (Foster et al., 2003), and intestine (Vallance et al., 2005). On the contrary, injuries to the heart, nervous system, and kidney are structurally and functionally irreversible, and fibrosis and scarring-the formation of connective tissue by fibroblasts, myofibroblasts, and immune cells-are the main contributors to the repair of these injured organs (Anders, 2012; Kawano et al., 2012; Deb and Ubil, 2014). In particular, astroglia primarily advance fibrosis,

which leads to glial scars in the central nervous system, and they prevent axonal regeneration by acting as physical barriers (Kawano et al., 2012).

Ischemia, some toxins, and trauma caused by accidents or surgical procedures can be triggers for tissue injury in the kidney. The renal repair process has been analyzed primarily by using experimental models for acute kidney injury (AKI), defined in human beings as the rapid reduction of renal function within 48 h (Moreno et al., 2011; Sohotnik et al., 2013; Thomas et al., 2015). In mice, the injection of high-dose folic acid (FA) is commonly used to induce AKI (Long et al., 2008). Although AKI mice show activated proliferation of renal tubular epithelial cells to repair injured tubules 2 days after FA injection, tubulointerstitial lesions characterized by interstitial fibrosis and tubule atrophy eventually appear a few weeks post-injection and thereafter (Long et al., 2008). This outcome emphasizes that renal injury is not fully repaired due to the limited functions of renal progenitor cells and the progression of tubulointerstitial lesions. Understanding the renal repair process through detailed analysis of animal models, with particular focus on fibrosis formation leading to irreversible renal dysfunction, is central to the development of effective therapies for kidney injury.

The activated cell proliferation induced by parenchymal progenitor cells, detected as bromodeoxyuridine (BrdU)-labeled cells (Maeshima et al., 2003), is mainly observed in the proximal tubular epithelium (Yang et al., 2014), and repair features are rarely observed in other nephron components such as distal tubules and glomeruli, which are the regulation centers for urine production, blood pressure, and electrolytes (Yang et al., 2014). Therefore, repeated or continuous tubular injuries caused by renal diseases including AKI increase the risk for future chronic kidney disease (Thomas et al., 2015), the progression of which eventually leads to end-stage renal failure characterized by severe interstitial fibrosis that requires dialysis or renal transplantation. The formation of interstitial lesions is a repair response in injured kidneys; however, excessive interstitial fibrosis causes progressive loss of kidney function (Badid et al, 2000; Sugimoto et al., 2007). Therefore, early treatments to inhibit the signals for tubulointerstitial lesion formation are effective therapies in both human and veterinary medicine (Qi et al., 2006; Sugimoto et al., 2007).

Notably, the MRL/MpJ mouse strain, an inbred strain originating from C57BL/6J (0.3%), C3H/HeDi (12.1%), AKR/J (12.6%), and LG/J (75.0%) strains, shows a specific "wound-healing" phenotype in several organs (Gourevitch et al., 2003). The MRL/MpJ strain and its mutant, MRL/MpJ-lpr/lpr, are commonly used as models for autoimmune diseases (Kamogawa et al., 2002), and the results of a previous study demonstrated that punched holes in the pinnae of MRL/MpJ mice close completely without scarring (Gourevitch et al., 2003). In addition, MRL/MpJ mice show unique repair capabilities in heart tissue (Leferovich et al., 2001) and the central nervous system (Hampton et al., 2004). Briefly, compared with that in C57BL/6 mice, cryogenically injured heart tissue in MRL/MpJ mice shows markedly reduced scar formation and increased cardiac cell mitosis (Leferovich et al., 2001). Thus, MRL/MpJ mice are a useful model with which to seek crucial leads for the development of regenerative medicine for several organs. This unique repair capability in MRL/MpJ mice is closely related to the altered function or expression of several molecules associated with the cell cycle, proliferation, immune response, and extracellular matrix (Gourevitch et al., 2003; Bedelbaeva et al., 2010). Furthermore, MRL/MpJ mice carry approximately 20 genetic loci associated with ear-punched hole closure (Masinde et al., 2001). However, no reports have been published about the repair process in MRL/MpJ mouse kidneys.

Therefore, we hypothesized that MRL/MpJ mice have unique repair capabilities in their kidneys and that the elucidation of the pathological features of injured MRL/MpJ kidneys would contribute to understanding of the renal repair process. In this study, we analyzed the formation of tubulointerstitial lesions after the induction of AKI or traumatic kidney injury (TKI) to compare the renal repair processes of MRL/MpJ mice and C57BL/6 mice, which have been used in previous studies as comparative controls in evaluations of the repair capabilities of the central nervous system and heart.

Materials and methods

Animals and sample preparation

We adhered to the *Guide for the Care and Use of Laboratory Animals of Hokkaido University, Graduate School of Veterinary Medicine* (approved by the Association for Assessment and Accreditation of Laboratory Animal Care International). Male C57BL/6 and MRL/MpJ mice aged 9-12 weeks were bred under specific pathogen-free conditions in the laboratory. For sample preparation, all experimental mice were killed via the cutting of the carotid artery under deep anesthesia induced with intraperitoneally administered 2,2,2-tribromoethanol dissolved in 2-methyl-2-butanol (Avertin, 2,400 mg/kg; Sigma-Aldrich, St. Louis, Missouri, USA). The kidneys and serum were collected immediately. Two hours before collection, BrdU (Wako, Osaka, Japan) in vehicle (0.01 M phosphate-buffered saline) was injected into the mice intraperitoneally at a dose of 50 mg/kg body weight.

Blood biochemistry

The levels of serum blood urea nitrogen (BUN) and creatinine (Cr) were measured with Fuji Drichem (Fujifilm Medical Co. Ltd., Tokyo, Japan) at the Japan Food Research Laboratories (Hokkaido, Japan).

FA-induced AKI model

Male C57BL/6 and MRL/MpJ mice aged 9-12 weeks were used. FA (Sigma-Aldrich) in vehicle (0.2 mL of 0.3 M $NaHCO_3$) was administered intraperitoneally to the mice at a dose of 250 mg/kg body weight according to the procedure of Gupta et al. (2012). As a control group, some mice received vehicle alone. The mice were killed 1, 2, 7, or 14 days after FA injection, and the kidneys and serum were collected.

TKI model

Ten-week-old male C57BL/6 and MRL/MpJ mice were used. Under deep anesthesia (Avertin, 1,500 mg/kg, administered intraperitoneally), the right kidney was antiseptically drawn out of the abdominal cavity. Then, to imitate renal biopsy, a flame-sterilized 22-G needle was inserted approximately 5 mm from the lateral border to the hilum. After hemostasis, the incised wound was closed antiseptically, and the mice were recovered on a warm table. Mice were killed 7 or 60 days post-injury (dpi), and the right and left kidneys were collected as injured and control kidneys, respectively. No infectious lesions were observed in any of the mice after the procedure.

Histological analysis

The kidney samples for histology were fixed with 4% paraformaldehyde/0.1 M phosphate buffer at 4°C overnight. Paraffin sections (2-μm thick) were then prepared and stained with periodic acid-Schiff (PAS). PAS-stained sections from AKI model kidneys were used to evaluate renal tubular injuries semi-quantitatively under a light microscope at 200× magnification. The degree of renal tubular injury was judged by the appearance of dilated and atrophied tubules, luminal casts, and deciduated epithelial cells and loss of brush border. Based on their severity, renal tubular injuries were scored on a scale of 1 to 5 as follows: 0=no tubular injury; 1≤10% of tubules injured; 2=10-25% of tubules injured; 3=26-50% of tubules injured; 4=51-75% of tubules injured; 5≥75% of tubules injured. More than 5 fields were scored, and the average was used as a measurement value in a mouse. In the TKI model, paraffin sections (2-μm thick) were prepared and stained with Masson's trichrome (MT). Paraffin sections (5-μm thick) were also prepared and stained with Von Kossa (VK).

Immunostaining

The kidney samples for histology were fixed with 4% paraformaldehyde/0.1 M phosphate buffer at 4°C overnight. Paraffin sections (3-μm thick) were then prepared and stained with immunohistochemistry for interleukin 1 family member 6 (IL-1F6), kidney injury molecule 1 (KIM-1; also known as hepatitis A virus cellular receptor 1 or TIM-1), alpha smooth muscle actin (αSMA), F4/80, CD3, and B220 to detect injured distal tubules, injured proximal tubules, myofibroblasts, macrophages, T cells, and B cells, respectively. For the AKI model, the immunohistochemistry for transforming

Table 1. Primary and secondary antibodies used in this study.

Antibody	Host	Dilution	Source	Antigen retrieval	Blocking
αSMA	Rabbit	1:3000	Abcam, Cambridge, UK	CB 20 min at 105°C	10% NGS
B220	Rat	1:1600	Cedarlane, Burlington, Ontario, Canada	0.1% pepsin/0.2 M HCl 5 min at 37°C	10% NGS
BrdU	Rat	1:100	Abcam	CB 20 min at 105°C	0.25% casein
Calbindin-D-28K	Rabbit	1:250	Spring Bioscience, Pleasanton, California, USA	CB 20 min at 105°C	0.25% casein
CD3	Rabbit	1:150	Nichirei, Tokyo, Japan	CB 15 min at 105°C	10% NGS
F4/80	Rat	1:500	Abcam	CB 5 min at 105°C	10% NGS
Hnf4α	Goat	1:400	Santa Cruz Biotechnology, Dallas, Texas, USA	CB 20 min at 105°C	0.25% casein
IL-1F6	Goat	1:400	R&D Systems, Minneapolis, Minnesota, USA	CB 20 min at 105°C	10% NDS
KIM-1	Rabbit	1:200	Santa Cruz Biotechnology	CB 20 min at 90°C	10% NGS
MMP-2	Mouse	1:300	Abcam	CB 15 min at 105°C	MOUSESTAIN KIT (Nichirei)
TGF-β1	Rabbit	1:100	Santa Cruz Biotechnology	Tris 15 min at 105°C	10% NGS
Goat IgG-Alexa Fluor 488	Donkey	1:500	Life Technologies, Carlsbad, California, USA		
Goat IgG-biotinylated	Donkey	1:100	Santa Cruz Biotechnology		
Simple Stain Mouse Max PO	-	Undiluted	Nichirei		
Rabbit IgG-biotinylated	Goat	Undiluted	Nichirei		
Rabbit IgG-Alexa Fluor 350	Donkey	1:500	Life Technologies		
Rat IgG-biotinylated	Goat	1:100	Caltag-Medsystems Limited, Buckingham, UK		
Rat IgG-TRITC	Goat	1:100	Rockland, Limerick, Pennsylvania, USA		

αSMA, alpha small muscle actin; BrdU, bromodeoxyuridine; CB, 10 mM citrate buffer (pH 6.0); Hnf4α, hepatocyte nuclear factor 4 alpha; Ig, immunoglobulin; IL, interleukin; KIM-1, kidney injury molecule 1; MMP-2, matrix metalloproteinase 2; NDS, normal donkey serum; NGS, normal goat serum; TGF-β1, transforming growth factor beta 1; TRITC, tetramethylrhodamine isothiocyanate; Tris, 20 mM Tris-HCl (pH 8.0).

growth factor beta 1 (TGF-β1) and matrix metalloproteinase 2 (MMP-2) was also performed, and each immunoglobulin G (IgG) isotype control (Santa Cruz Biotechnology, Dallas, Texas, USA) was used as the negative control. Briefly, the paraffin sections were deparaffinized and antigen-retrieved. After cooling, the slides were soaked in methanol containing 3% H_2O_2 for 20 min at room temperature to remove internal peroxidase. After being washed, the sections were blocked with each reagent for 60 min at room temperature and incubated with primary antibodies overnight at 4°C. After 3 washings with phosphate-buffered saline, the sections were incubated with secondary antibodies for 30 min at room temperature, washed again, and incubated with streptavidin-biotin complex (SABPO[R] kit; Nichirei, Tokyo, Japan) for 30 min. The sections were then incubated with 3,3′-diaminobenzidine tetraydrochloride-H_2O_2 solution. Finally, the sections were slightly counterstained with hematoxylin. The details of the antigen retrieval, dilution, and antibodies used are shown in Table 1.

Immunofluorescence for BrdU, hepatocyte nuclear factor 4 alpha (HNF4α), and calbindin-D-28K was performed to detect proliferating cells, proximal tubules, and distal convoluted tubules, respectively. After overnight incubation with primary antibodies at 4°C, each section was incubated with secondary antibodies for 1 h at room temperature. The sections were observed under a fluorescence microscope (BZ-9000, Keyence, Osaka, Japan). The details of the antigen retrieval, dilution, and antibodies used are shown in Table 1.

Histoplanimetry

For the quantification of KIM-1-, IL-1F6-, and BrdU-positive reactions, positive tubules (KIM-1, IL-1F6) or cells (BrdU) per unit area of kidney were counted at 400× magnification (KIM-1) and 200× magnification (IL-1F6, BrdU). More than 5 fields were measured, and the average was expressed as the number per area (mm^2) and used as a measurement value in a mouse.

For determination of the indices of renal fibrosis in TKI model kidneys, digital images of the kidney sections stained with MT at 400× magnification were prepared for each mouse. The blue-stained area was measured with ImageJ ver. 1.48 (National Institutes of Health, Bethesda, Maryland, USA) in a 0.011-mm^2 area centered on the injured region. Similarly, in TKI models, the black areas on VK-stained sections and the brown areas on immunostained sections were measured with ImageJ in the total area of the kidney section centered on the injured region to determine indices of calcification and αSMA expression, respectively.

Reverse transcription and quantitative polymerase chain reaction

For messenger RNA (mRNA) expression examination, total RNAs were purified from kidneys stored in RNAlater solution (Ambion/Applied Biosystems, Carlsbad, California, USA) using the TRIzol® Reagent (Ambion) according to the manufacturer's protocol. DNase-treated total RNAs were synthesized to complementary DNAs via reverse transcription with the GoScript™ reaction (Promega, Madison, Wisconsin, USA). Each complementary DNA, adjusted to 100 μg/mL, was used for quantitative polymerase chain reaction with Brilliant III Ultra-Fast SYBR® Green QPCR Master Mix (Agilent, Santa Clara, California, USA). The sequences of the primer pairs used in this study are shown in Table 2.

Statistical analysis

The results were expressed as means ± standard error and statistically analyzed using a non-parametric Mann-Whitney U-test ($P<0.05$).

Results

Renal pathology in FA-induced AKI model mice

Fig. 1 shows the changes in histopathology and renal function in FA-induced AKI model mouse kidneys. In both C57BL/6 and MRL/MpJ mouse kidneys, the dilation and atrophy of renal tubules with PAS-positive protein casts were commonly observed beginning 1 day after FA injection (Fig. 1C-J). Beginning on day 7, some tubular epithelial cells detached and lost their brush borders, and mononuclear cells infiltrated around them (Fig. 1G-J). No significant strain difference was observed in the formation of tubulointerstitial lesions during the observation period, and the histopathological scores of renal injury changed similarly in both strains,

Table 2. Specific gene primers used in this study.

Gene (accession no.)	Primer sequence (5′-3′)		Product size (bp)
Actb (NM_007393)	Forward	TGTTACCAACTGGGACGACA	165
	Reverse	GGGGTGTTGAAGGTCTCAAA	
Il6 (NM_031168)	Forward	TGTATGAACAACGATGATGCAC	137
	Reverse	TGGTACTCCAGAAGACCAGAGG	
Mmp2 (NM_008610)	Forward	GGCTGGAACACTCTCAGGAC	212
	Reverse	CGATGCCATCAAAGACAATG	
Mmp9 (NM_013599)	Forward	TGGGTGTACACAGGCAAGAC	199
	Reverse	ACTCCTTATCCACGCGAATG	
Sod1 (NM_011434)	Forward	GAACCATCCACTTCGAGCAG	173
	Reverse	GCCACCATGTTTCTTAGAGTGAG	
Tgfb1 (NM_009370)	Forward	ACCTTCTGATCCATCGGTTG	202
	Reverse	TTCCTGTTGGCTGAGTTGTG	

Actb, actin, beta; Bmp, bone morphogenic protein; Il6, interleukin 6; Mmp, matrix metalloproteinase; Sod1, superoxide dismutase 1, soluble; Tgfb1, transforming growth factor beta 1.

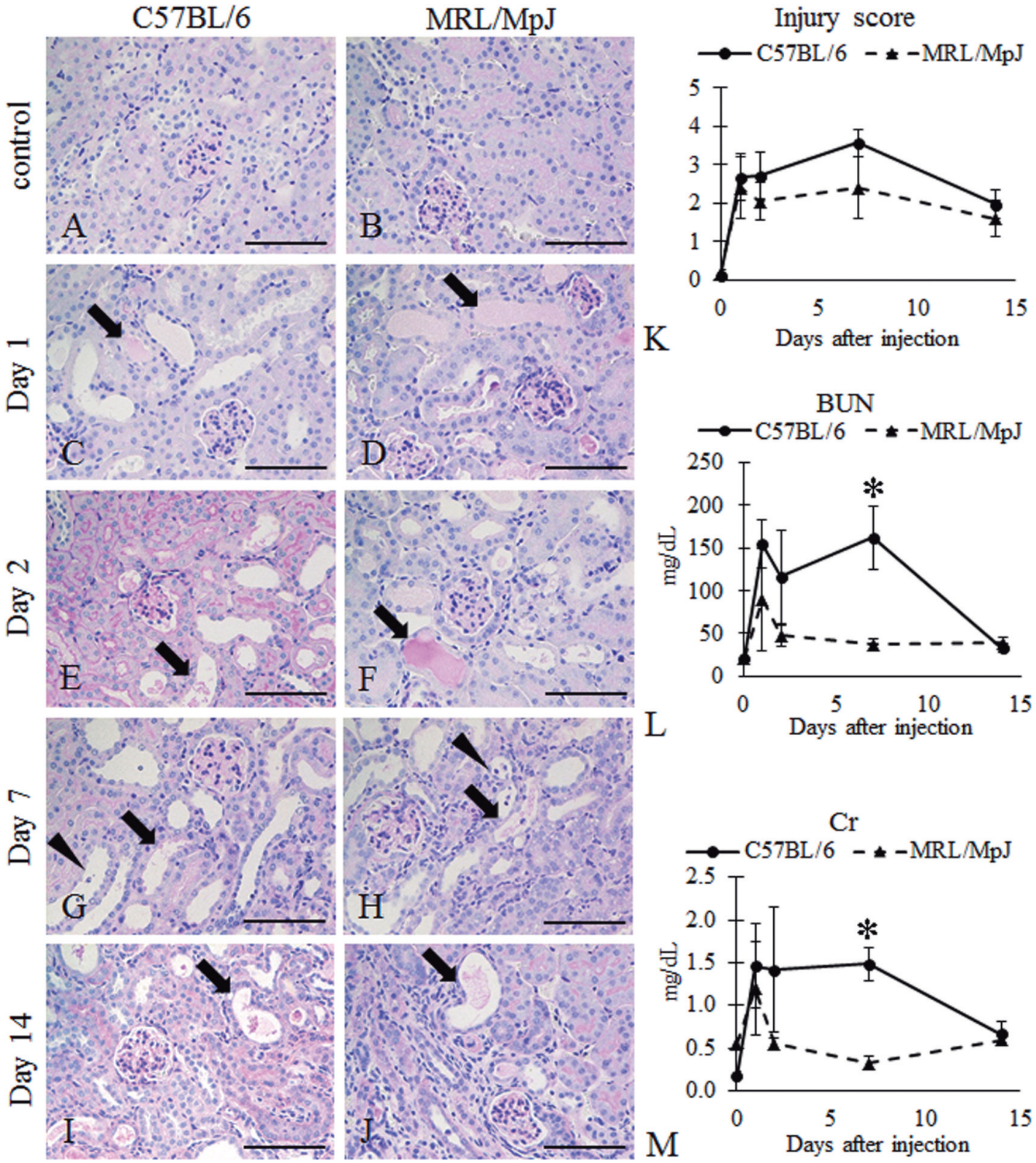

Fig. 1. Renal pathology and function in folic acid (FA)-induced acute kidney injury (AKI) models. **A-J.** Renal cortices of C57BL/6 and MRL/MpJ mouse kidneys after FA-induced AKI. Renal cortices of control kidneys show normal histology in both strains **(A and B)** at day 0. After FA injection, the dilation and atrophy of renal tubules with periodic acid-Schiff (PAS)-positive casts (arrows) are similar in the kidneys of both strains at day 1 **(C-J)**. Detached tubular epithelial cells (arrowheads) are noted at day 7 after FA injection in both strains **(G and H)**. PAS staining. **K-M.** Histoplanimetrical scores of kidney injury and serum blood urea nitrogen (BUN) and creatinine (Cr) levels in C57BL/6 and MRL/MpJ mice after FA-induced AKI. n≥3. Values=means ± standard error (SE). *Significant difference between C57BL/6 and MRL/MpJ mouse kidneys at the same time points after AKI induction ($P<0.05$, Mann-Whitney U-test). Scale bars: 100 μm.

although these scores increased after FA injection (Fig. 1K). On the contrary, serum BUN and Cr levels in MRL/MpJ mice were lower than those of C57BL/6 mice after FA injection, and significant difference was observed at day 7 (Fig. 1L,M).

Renal tubular injuries in FA-induced AKI model mice

To evaluate renal tubular injuries in FA-induced AKI model mouse kidneys, we performed immunohistochemistry for KIM-1 and IL-1F6 to detect injured

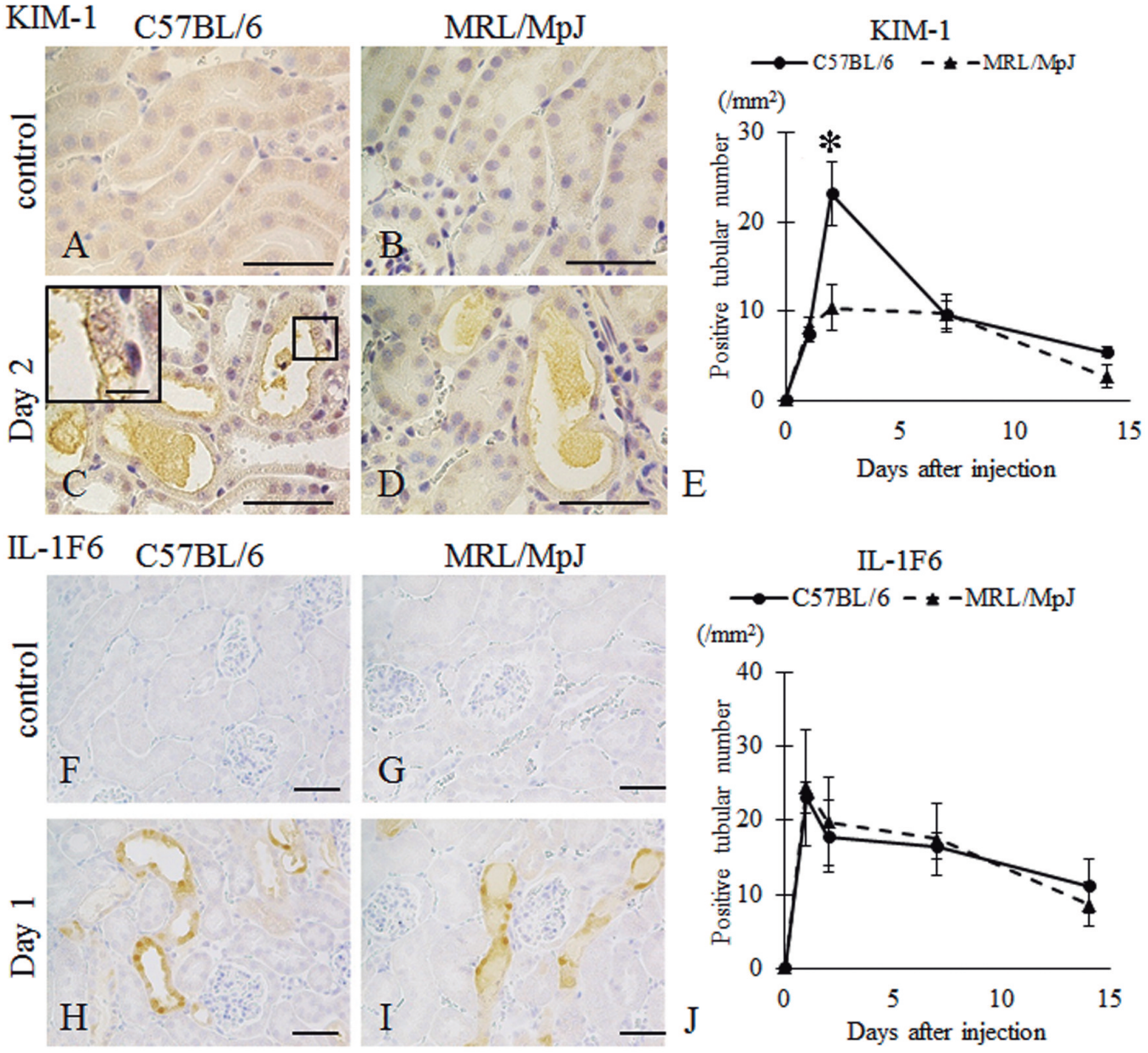

Fig. 2. Tubular damage in FA-induced AKI model kidneys. **A-D.** Immunohistochemistry for kidney injury molecule 1 (KIM-1) as a proximal tubular damage marker in the kidneys of C57BL/6 and MRL/MpJ mice after FA-induced AKI. No positive reaction occurred at day 0 in the control kidneys of either strain **(A and B)**. After FA injection, KIM-1-positive reactions were observed in the apical portion of epithelial cells in the dilated tubules of both strains **(C and D)**. The extended image is shown in panel C (square). **E.** Number of KIM-1-positive tubules in C57BL/6 and MRL/MpJ mouse kidneys after FA-induced AKI. n≥3. Values=means ± SE. *Significant difference between C57BL/6 and MRL/MpJ mouse kidneys ($P<0.05$, Mann-Whitney U-test). **F-I.** Immunohistochemistry for interleukin 1 family member 6 (IL-1F6) as a distal tubular damage marker in C57BL/6 and MRL/MpJ mouse kidneys after FA-induced AKI. No positive reaction was observed at day 0 in the control kidneys of either strain **(F and G)**. After FA injection, IL-1F6-positive reactions were observed in the cytoplasm and nuclei of the dilated tubules of both strains **(H and I)**. **J.** Number of IL-1F6-positive tubules in C57BL/6 and MRL/MpJ mouse kidneys after FA-induced AKI. n≥3. Values=means ± SE. *Significant difference between C57BL/6 and MRL/MpJ mouse kidneys at the same time point ($P<0.05$, Mann-Whitney U-test). Scale bars: 50 μm; Insert in C, 10 μm.

proximal and distal tubules, respectively. No positive reactions for KIM-1 and IL-1F6 were observed in the control C57BL/6 and MRL/MpJ mouse kidneys (Fig. 2A,B,F,G). On the contrary, positive reactions for KIM-1 and IL-1F6 were observed in the apical portion of tubular epithelial cells and the cytoplasm, nuclei, or both of dilated tubules, respectively, in AKI model mouse kidneys (Fig. 2C,D,H,I). For histoplanimetry in both strains, the number of KIM-1- and IL-1F6-positive tubules increased, with peaks at days 1 and 2 after FA injection, respectively (Fig. 2E,J). The number of KIM-1-positive tubules in MRL/MpJ mouse kidneys was significantly lower than that in C57BL/6 mouse kidneys at day 2 after FA injection (Fig. 2E). By contrast, no significant difference in the number of IL-1F6-positive tubules was observed between the strains throughout the observation period (Fig. 2J).

Next, we quantified the mRNA expression of interleukin 6 (*Il6*) and superoxide dismutase 1, soluble (*Sod1*), which encode a representative inflammatory cytokine via nuclear factor kappa B (NFκB) signaling and an antioxidant enzyme (Sivakumar et al., 2010), respectively, in FA-induced AKI model mouse kidneys (Fig. 3). *Il6* mRNA expression increased significantly at day 7 after AKI induction in C57BL/6 mice (Fig. 3A). MRL/MpJ mice also tended to show increased *Il6* mRNA expression after AKI, but no statistical significance was found. Compared with C57BL/6 mice, MRL/MpJ mice showed significantly higher *Sod1* mRNA expression at day 0 after AKI (Fig. 3B). However, at day 7 after AKI, *Sod1* mRNA expression significantly increased after AKI in C57BL/6 mice, but no increase was observed in MRL/MpJ mice.

Renal histopathology in TKI model mouse kidneys

The histopathology results for the FA-induced AKI model kidneys indicated pathological differences between C57BL/6 and MRL/MpJ mice in renal function changes and proximal tubular injuries. We also observed differences in the renal repair processes of the 2 strains after TKI induced by needle puncture, perhaps because FA model mice are also affected by pharmacological differences between the strains. At 7 dpi, the injured area was occupied by PAS-positive necrotizing tubules that extended to the border between normal tissue and the injured area (Fig. 4A-D). No strain-related histopathological difference was observed at 7 dpi. At 60 dpi, the center of the injured area was replaced by scars, and a strain-related difference was observed at the border between normal tissue and the injured area (Fig. 4E-H). Briefly, the fibrotic tissue increased with the increase in extracellular matrix in C57BL/6 mouse kidneys but was scarce in MRL/MpJ mouse kidneys. Furthermore, PAS-positive tubule-like structures were observed in MRL/MpJ mouse kidneys and appeared calcified.

Renal fibrosis in TKI model mouse kidneys

Fibrosis after TKI was compared between the strains by using MT-stained sections. Aniline blue-positive fibrotic areas were observed at the border between normal tissue and the injured area at 7 dpi in C57BL/6 mouse kidneys but were scarcely observed in MRL/MpJ mouse kidneys (Fig. 5A-D). At 60 dpi, the fibrotic areas increased in both strains, but that in C57BL/6 mouse kidneys was larger. The results of histoplanimetry showed that the percentage of the fibrotic area in C57BL/6 mouse kidneys was higher than that in MRL/MpJ mouse kidneys at 7 and 60 dpi, and significant difference was observed at 60 dpi (Fig. 5E).

Furthermore, the appearance of myofibroblasts, which secrete extracellular matrix (Badid et al., 2000), was examined with immunohistochemistry for αSMA (Fig. 6). At 7 and 60 dpi, αSMA-positive cells were observed at the walls of vessels or at the border between normal tissue and the injured area in C57BL/6 mouse kidneys, and their numbers seemed to be higher at 7 dpi than at 60 dpi (Fig. 6A,C). On the contrary, these positive reactions were mainly observed at the walls of

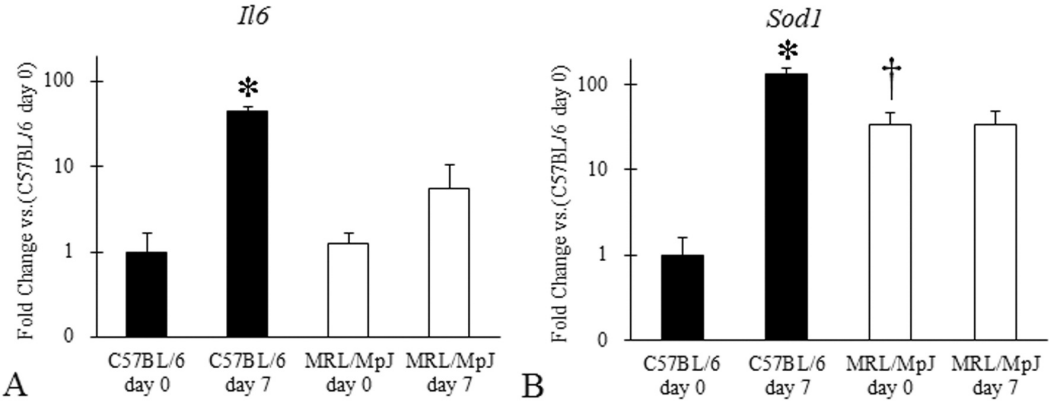

Fig. 3. Messenger RNA (mRNA) expression levels of an inflammatory cytokine and an antioxidative enzyme in AKI model kidneys. **A.** mRNA expression levels of interleukin 6 (Il6) in C57BL/6 and MRL/MpJ mouse kidneys after AKI. **B.** mRNA expression levels of superoxide dismutase 1, soluble (Sod1) in C57BL/6 and MRL/MpJ mouse kidneys after AKI. n≥4. Values=means ± SE. *Significant difference between results at day 0 and day 7 after AKI (P<0.05, Mann-Whitney U-test). †Significant difference between C57BL/6 and MRL/MpJ mice at the same time point (P<0.05, Mann-Whitney U-test).

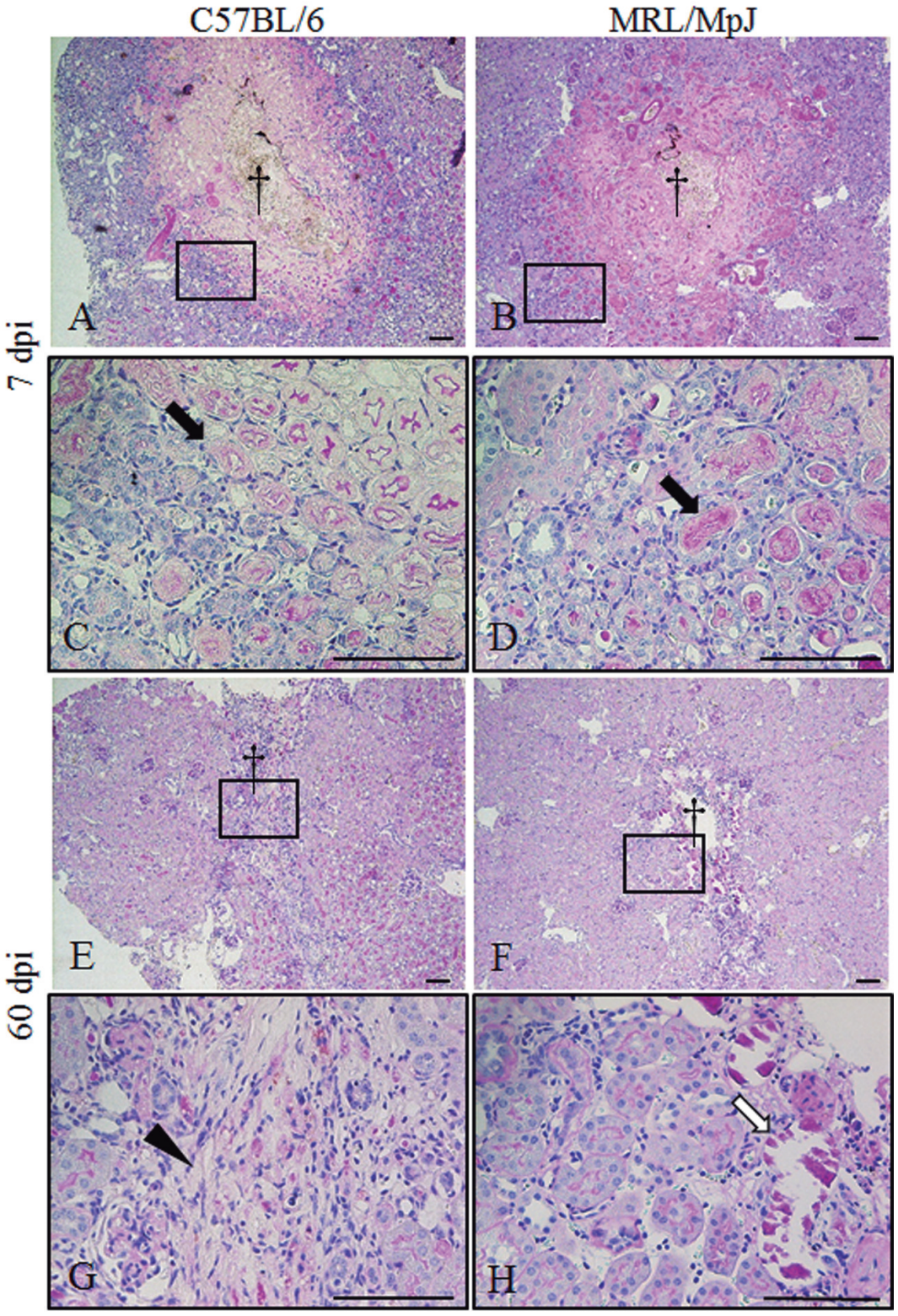

Fig. 4. Renal pathology in traumatic kidney injury (TKI) model kidneys. **A-D.** Renal cortices at 7 days post-injury (dpi) after needle puncture in C57BL/6 and MRL/MpJ mouse kidneys. Injured areas in the kidneys of both strains are occupied by necrotizing tubules **(A and B)**, and their centers (**A and B**, daggers) contain erythrocytes. Necrotizing tubules are clearly observed in the squares in A and B (**C and D**, arrows). PAS staining. **E-H.** Renal cortices at 60 dpi after needle puncture in C57BL/6 and MRL/MpJ mouse kidneys. The necrotic lesions in the injured areas of both strains at 60 dpi **(E and F)** are milder than those at 7 dpi (**A-D**). In tubulointerstitial lesions around the punctured areas (**E and F**, squares), increased fibrotic tissues with extracellular matrix (**G**, arrowhead) and PAS-positive tubule-like structures (**H**, white arrow) are seen in the tubulointerstitial tissue of C57BL/6 and MRL/MpJ mouse kidneys. Daggers denote the centers of the punctured areas. PAS staining. Scale bars: 100 μm.

vessels in MRL/MpJ mouse kidneys (Fig. 6B,D). The histoplanimetry results showed that the percentage of the αSMA-positive area in C57BL/6 mouse kidneys was significantly higher than that in MRL/MpJ mouse kidneys at 7 dpi.

Renal calcification in TKI model mouse kidneys

To detect calcification after TKI, as shown in Fig. 4H, we performed VK calcium staining. At 7 dpi, calcification was detected at the border between normal and injured tissues only in MRL/MpJ mouse kidneys, and it became more remarkable compared with that in C57BL/6 mouse kidneys at 60 dpi (Fig. 7A-D). According to histological observations, the percentage of the calcified area was higher in MRL/MpJ mouse kidneys than in C57BL/6 mouse kidneys at 7 and 60 dpi, and significant difference was observed at 60 dpi (Fig. 7E).

Expression of candidate molecules for fibrosis or calcification in TKI model mouse kidneys

Compared with C57BL/6 mouse kidneys, MRL/MpJ mouse kidneys showed significantly smaller fibrotic areas and larger calcification areas histopathologically after TKI. To confirm this observation, we examined the mRNA expression of genes encoding molecules associated with the formation of fibrosis or calcification, such as *Tgfb1* (a cytokine that promotes organ fibrosis) and *Mmp2* and *Mmp9* (proteinases that degrade extracellular matrix). The fold change in expression was determined by comparing the degrees of change between expression levels in traumatically injured kidneys and baseline expression in the control kidneys of each strain. Although *Tgfb1* expression tended to be increased in both strains at 7 dpi, significant difference was observed only in C57BL/6 mouse kidneys (Fig. 8A). No strain-related difference in *Tgfb1* expression was observed at 60 dpi (Fig. 8D). *Mmp2* expression increased in both strains at 7 dpi and only in MRL/MpJ mouse kidneys at 60 dpi (Fig. 8B,E). There was no significant difference in *Mmp9* expression in either strain at 7 and 60 dpi (Fig. 8C,F).

Immunohistochemically, TGF-β1-positive reactions were detected in the cytoplasm of damaged renal tubules around the punctured area in both strains at 7 dpi (Fig 8G,H), but these reactions seemed to be weaker in

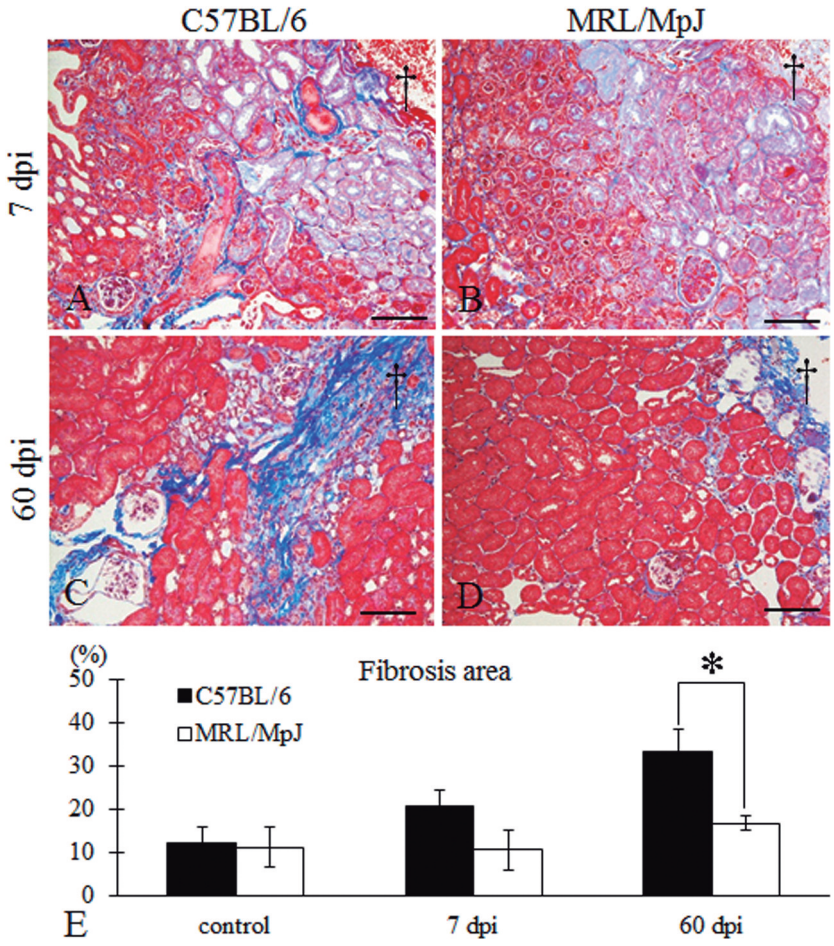

Fig. 5. Fibrosis in TKI model kidneys. **A-D.** Renal cortices of C57BL/6 and MRL/MpJ mouse kidneys after TKI. At 7 dpi, aniline blue-positive areas appear at the borders between normal tissue and injured areas in C57BL/6 mouse kidneys **(A)** but are scarcely observed in MRL/MpJ mouse kidneys **(B)**. Fibrotic areas at 60 dpi are increased compared with those at 7 dpi in both strains, and compared with C57BL/6 mouse kidneys **(C)**, MRL/MpJ mouse kidneys **(D)** have smaller fibrotic areas. Daggers denote the punctured areas. Masson's trichrome staining. **E.** Histoplanimetrical scores for fibrotic areas in the kidneys of C57BL/6 and MRL/MpJ mice after TKI. n=4. Values=means ± SE. *Significant difference between C57BL/6 and MRL/MpJ mouse kidneys at the same time point ($P<0.05$, Mann-Whitney U-test). Scale bars: 100 μm.

MRL/MpJ mice. At 60 dpi, TGF-β1-positive reactions decreased in both strains, although nonspecific reactions, which were checked with isotype IgG control staining (data not shown), were observed in calcified lesions (Fig. 8I,J). MMP-2-positive reactions were detected in the cytoplasm of damaged renal tubules around the punctured area in both strains at 7 dpi (Fig. 8K,L), but these reactions seemed to be weaker in MRL/MpJ mice. Although MMP-2-positive reactions decreased in both strains at 60 dpi, MMP-2-positive mononuclear cells were observed at the tubulointerstitium around the punctured area in MRL/MpJ mice (Fig. 8M). These reactions were not observed with isotype IgG control staining (Fig. 8N).

Cell proliferation and infiltration in TKI model mouse kidneys

To investigate cell proliferation in TKI, we performed immunofluorescence for BrdU, Hnf4α, and calbindin-D-28K to detect proliferating cells and proximal and distal convoluted tubular epithelial cells, respectively (Fig. 9A,B). BrdU-positive reactions were observed in the nuclei of tubular epithelial cells and mononuclear cells in the renal interstitium of both strains. Hnf4α- and calbindin-D-28K-positive cells were detected in the nuclei and cytoplasm, respectively, of tubular cells in both strains, and some positive cells for Hnf4α but not calbindin-D-28K also showed BrdU-

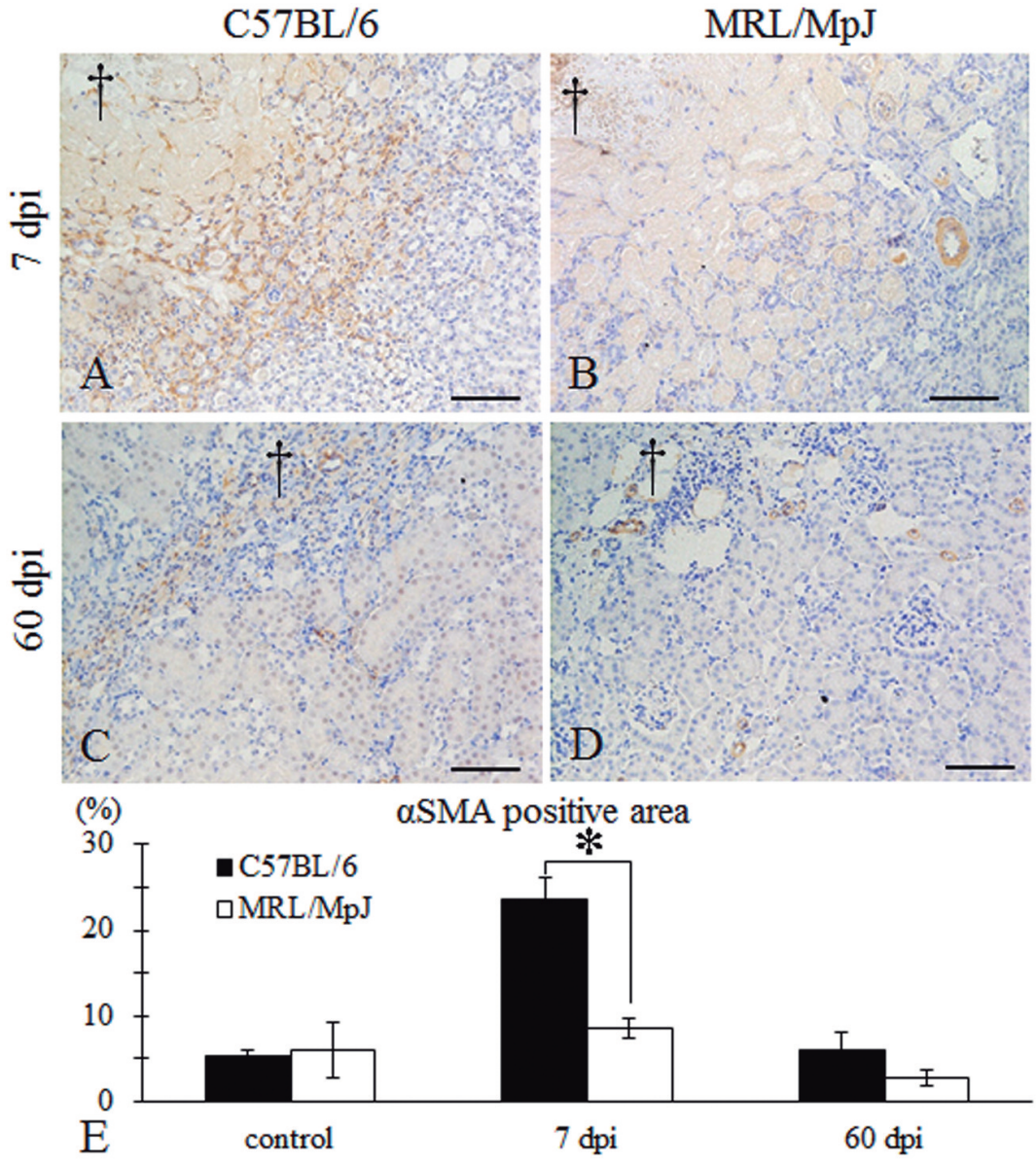

Fig. 6. Appearance of myofibroblasts in TKI model kidneys. **A-D.** Immunohistochemistry for alpha small muscle actin (αSMA) as a marker of myofibroblasts in C57BL/6 and MRL/MpJ mouse kidneys after TKI. αSMA-positive cells are present between normal tissues and the injured areas, and their number at 7 dpi **(A)** seems to be higher than that at 60 dpi in C57BL/6 mouse kidneys **(C)**. αSMA-positive cells are mainly detected in vessel walls at 7 dpi **(B)** and 60 dpi **(D)** in MRL/MpJ mouse kidneys. Daggers denote the punctured areas. **E.** Histoplanimetrical scores for αSMA-positive areas in C57BL/6 and MRL/MpJ mouse kidneys after TKI. n=4. Values=means ± SE. *Significant difference between C57BL/6 and MRL/MpJ mouse kidneys at the same time point ($P<0.05$, Mann-Whitney U-test). Scale bars: 100 μm.

positive reactions in their nuclei. Histoplanimetry for cells positive for BrdU, Hnf4α, calbindin-D-28K, or a combination thereof showed no significant strain-related differences in the number of 3 kinds of cells: $BrdU^+/Hnf4\alpha^-/calbindin\text{-}D\text{-}28K^-$ proliferating interstitial cells, $BrdU^+/Hnf4\alpha^+/calbindin\text{-}D\text{-}28K^-$ proliferating proximal tubular epithelial cells, and $BrdU^+/Hnf4\alpha^-/calbindin\text{-}D\text{-}28K^+$ proliferating distal tubular epithelial cells (Fig. 9C). No $BrdU^+/Hnf4\alpha^-/calbindin\text{-}D\text{-}28K^+$ proliferating distal tubular epithelial cells were detected in either strain.

To observe the infiltration of inflammatory cells, we performed immunohistochemistry for F4/80, CD3, and B220 to detect macrophages, T cells, and B cells, respectively (Fig. 10). Many cells positive for F4/80, CD3, and B220 were detected around the injured areas at both 7 and 60 dpi, but no strain-related difference was found in the number of any cell type (Fig. 10A-L).

Discussion

KIM-1 is a representative marker of cell injury in proximal tubules, as reported in models of polycystic kidney disease, toxin-induced kidney injury, and ischemia-reperfusion kidney injury (Lim et al., 2013). In our FA-induced AKI model, no strain differences were found in the histopathological injury score and the number of IL-1F6-positive damaged distal tubules (Ichii et al., 2010), but compared with C57BL/6 mouse kidneys, MRL/MpJ mouse kidneys had fewer KIM-1-positive damaged proximal tubules. These data might indicate that epithelial cell damage to proximal tubules but not distal tubules was milder in MRL/MpJ mouse kidneys.

FA may injure the renal tubular epithelium through the formation of FA crystals (Long et al., 2008) and the induction of reactive oxygen species (Gupta et al., 2012), and harmful cytokines induced via NFκB signaling in the kidney may increase epithelial cell damage (Moreno et al., 2011). Notably, compared with C57BL/6 mouse tissues, MRL/MpJ mouse tissues including heart, liver, and regenerating ear hole reportedly show decreased levels of reactive oxygen species and oxidative phosphorylation (Naviaux et al., 2009). Furthermore, using cultured macrophages, we demonstrated that the induction of cytokines such as IL-

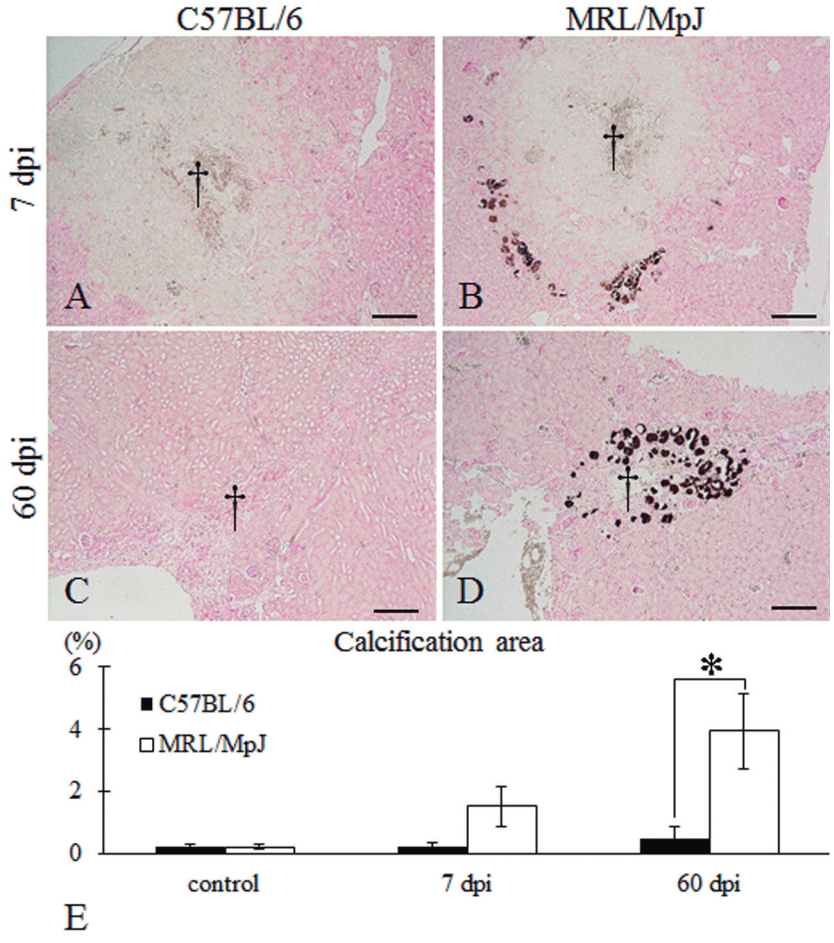

Fig. 7. Calcification in TKI model kidneys. **A-D.** Renal cortices of C57BL/6 and MRL/MpJ mouse kidneys after TKI. At 7 dpi, calcification (black area) between normal tissue and the injured area **(A)** is detected in MRL/MpJ mouse kidneys **(B)** but not in C57BL/6 mouse kidneys, and its difference becomes remarkable at 60 dpi **(C and D)**. Daggers denote the punctured areas. Von Kossa staining. **E.** Histoplanimetrical analysis for calcification areas in C57BL/6 and MRL/MpJ mouse kidneys after TKI. n=4. Values=means ± SE. *Significant difference between C57BL/6 and MRL/MpJ mouse kidneys at the same time point ($P<0.05$, Mann-Whitney U-test). Scale bars: 200 μm.

6 via NFκB signaling was weaker in MRL/MpJ mice than in C57BL/6 mice (Alleva et al., 1997). Interestingly, our results suggested that *Il6* mRNA induction was weaker in MRL/MpJ mouse kidneys than in the kidneys of C57BL/6 mice after AKI. Furthermore, the basal mRNA expression level of the antioxidant enzyme *Sod1* was higher in MRL/MpJ mouse kidneys than in C57BL/6 mouse kidneys, suggesting an antioxidative phenotype of MRL/MpJ mice. Thus, these characteristics of reactions to oxidative stress, cytokine expression, or both in MRL/MpJ mouse cells might decrease proximal tubular epithelium damage in FA-induced AKI. Indeed, the serum levels of BUN and Cr, clinical markers of renal dysfunction, in MRL/MpJ mice were lower than those in C57BL/6 mice, and this outcome was also associated with decreased damage to the proximal tubules in the former strain after FA-induced AKI.

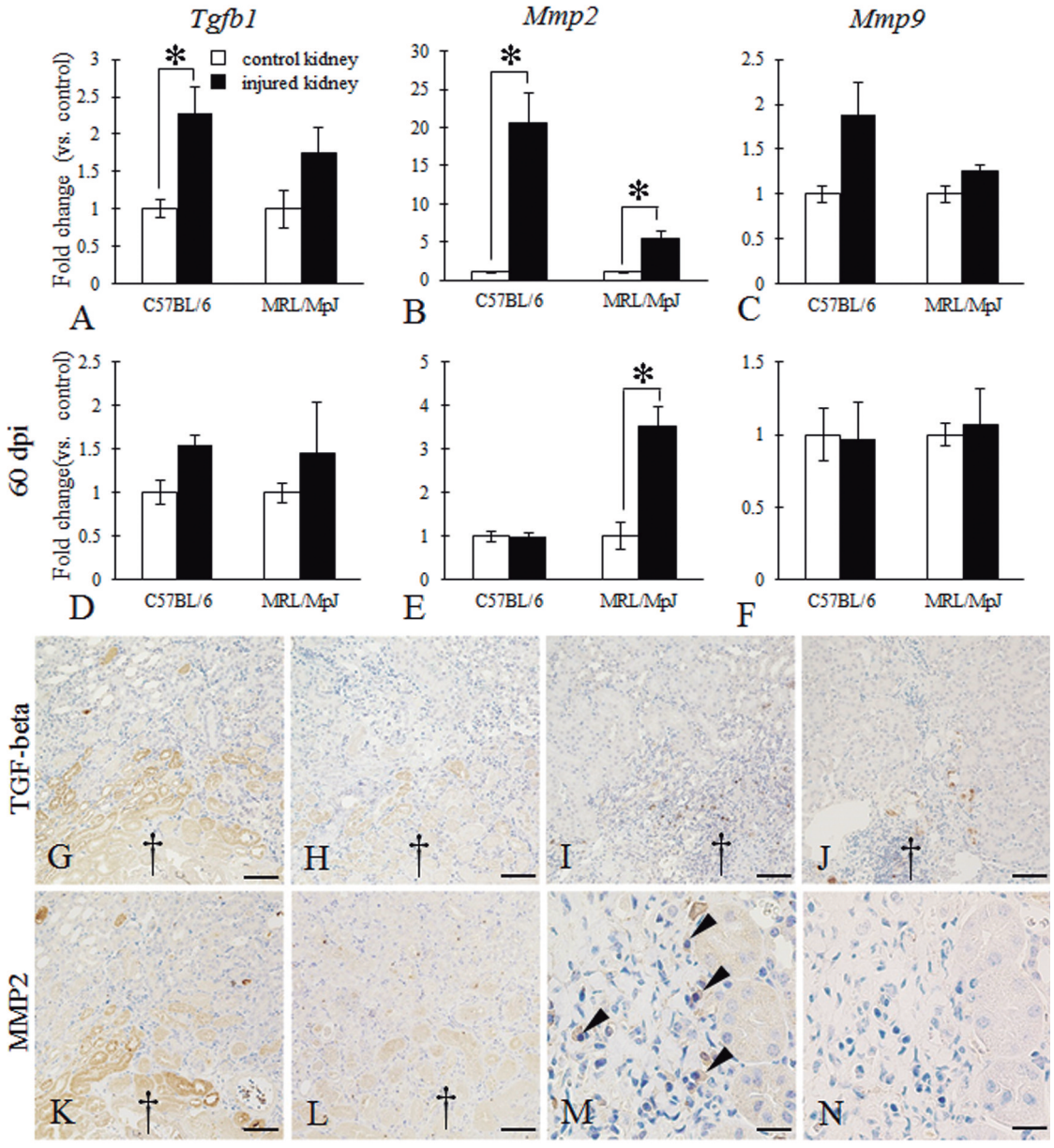

Fig. 8. mRNA expression levels of fibrosis- and calcification-related factors in TKI model kidneys. **A-F.** mRNA expression levels of fibrosis-related factors including transforming growth factor beta 1 (*Tgfb1*), matrix metalloproteinases 2 and 9 (*Mmp2* and *Mmp9*, respectively) in C57BL/6 and MRL/MpJ mouse kidneys after TKI. The fold change in expression was determined by comparing the degree of change between expression levels in traumatically injured kidneys and the baseline expression in the control kidneys of each strain. n≥3. Values=means ± SE. *Significant difference between control kidney and injured kidney ($P<0.05$, Mann-Whitney U-test). **G-N.** Immunohistochemistry for TGF-β1 and MMP-2 in C57BL/6 and MRL/MpJ mouse kidneys after TKI. At 7dpi, TGF-β1-positive reactions are observed in the cytoplasm of injured tubules around the punctured area (daggers) in the kidneys of C57BL/6 **(G)** and MRL/MpJ (**H**) mice. Compared with those at 7 dpi, TGF-β1-positive reactions at 60 dpi are decreased in C57BL/6 **(I)** and MRL/MpJ **(J)** mouse kidneys. At 7 dpi, MMP-2-positive reactions are observed in the cytoplasm of injured tubules around the punctured area (daggers) in the kidneys of C57BL/6 **(K)** and MRL/MpJ **(L)** mice. At 60 dpi, MMP-2-positive mononuclear cells are observed at the tubulointerstitium in MRL/MpJ mouse kidneys **(M)**. No positive reaction is observed in the immunoglobulin G isotype control staining **(N)**. Scale bars: 50 μm.

Strain differences observed in FA-induced AKI might be caused by the pharmacological differences between C57BL/6 and MRL/MpJ mouse kidneys. To investigate the renal repair process more directly, we induced TKI via needle puncture and observed significant strain difference in the histopathological analysis of MT-stained sections. The aniline blue-positive fibrotic area in MRL/MpJ mouse kidneys was smaller than that in C57BL/6 mouse kidneys. Interestingly, in other organs such as the ear (Gourevitch et al., 2003), heart (Leferovich et al., 2001), and central nervous system (Hampton et al., 2004), fibrotic activity in the former strain is induced less than it is in the latter. Therefore, we concluded that fibrotic activity in the kidneys of MRL/MpJ mice was lower than that in C57BL/6 mouse kidneys after TKI.

The detailed pathological process of renal fibrosis is still being debated. Injured renal tubular cells may produce cytokines, including TGF-β1, which then strongly induce the transformation of progenitor cells (i.e., erythropoietin-producing cells, pericytes, bone marrow cells, and tubular epithelial cells) to myofibroblasts that can produce extracellular matrix including collagens in tubulointerstitial regions (Mack and Yanagita, 2015). Compared with C57BL/6 mouse kidneys, MRL/MpJ mouse kidneys in the present study had fewer αSMA-positive myofibroblasts, lower mRNA expression of *Tgfb1*, and lower immune-positive TGF-β1 reactions, and these data also supported the lower fibrotic activity observed in MRL/MpJ mouse kidneys.

Furthermore, renal fibrosis is regulated by the balance between the accumulation and breakdown of extracellular matrix produced by myofibroblasts (Badid et al., 2000; Johnson et al., 2002); MMP-2 and MMP-9 (also known as gelatinases A and B, respectively), secreted mainly by the tubular cells in the kidneys (Cavdar et al., 2013), play key roles in the latter process. In C57BL/6 and MRL/MpJ mouse kidneys, the mRNA expression levels of *Mmp2* increased at 7 dpi. Importantly, only MRL/MpJ mouse kidneys retained the increased mRNA expression level of *Mmp2* at 60 dpi, and fibrosis with extracellular matrix was observed in C57BL/6 mouse kidneys at this time point. Mononuclear cells in the tubulointerstitium expressed MMP-2 in MRL/MpJ mouse kidneys at 60 dpi. Previous studies have suggested that compared with those of control mice, the ear holes and injured central nervous systems of MRL/MpJ mice show higher levels of MMP-2 activation (Gourevitch et al., 2003; Hampton et al.,

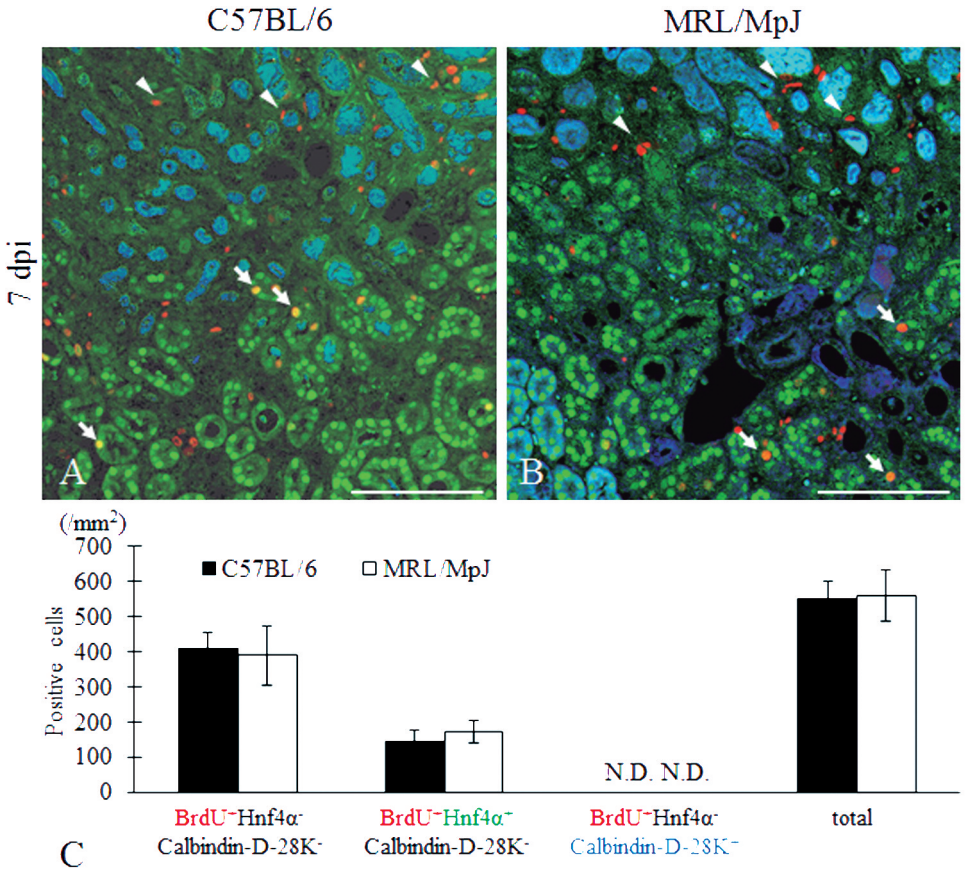

Fig. 9. Cell proliferation in TKI model kidneys. **A and B.** Immunofluorescence for bromodeoxyuridine (BrdU; proliferating cell marker), hepatocyte nuclear factor 4 alpha (Hnf4α; proximal tubule epithelial cell marker), and calbindin-D-28K (distal tubule epithelial cell marker) in C57BL/6 and MRL/MpJ mouse kidneys at 7 dpi after TKI. BrdU-positive reactions (red) are observed in nuclei of the tubular epithelium and mononuclear cells in the renal interstitium (red, arrowheads) in both strains. Hnf4α (green)- and calbindin-D-28K (blue)-positive reactions are observed in tubular nuclei and the cytoplasm of tubular cells, respectively. Some Hnf4α-positive cells but not calbindin-D-28K-positive cells show positive reactions for BrdU (yellow, arrows). **C.** Number of cells positive for BrdU, Hnf4α, calbindin-D-28K, or a combination thereof in C57BL/6 and MRL/MpJ mouse kidneys at 7 dpi after TKI. n=4. Values=means ± SE. N.D.: not detected. Scale bars: 100 μm.

2004). Therefore, the activated MMP-2 in the injured MRL/MpJ mouse kidneys may be associated with lower fibrotic activity due to the breakdown of extracellular matrix.

The results of this study provided no clear explanation for the comparatively lower fibrotic activity in MRL/MpJ mouse kidneys. However, this unique phenotype might be related to the response of tubular cells to injury rather than the regeneration of tubular cells, because no clear strain difference was observed in the proliferation of tubular cells after TKI in this study. MRL/MpJ mice carry approximately 20 genetic loci susceptible for ear-punched hole closure (Masinde et al., 2001), and some of these loci might help reduce fibrotic activity in the ear. Interestingly, p21-deficient mice and MRL/MpJ mice use similar mechanisms to close ear holes (Bedelbaeva et al., 2010). p21 is a cyclin-dependent kinase inhibitor that arrests the cell cycle, and compared to those of C57BL/6 mice, cultured fibroblast-like cells of MRL/MpJ mice show reduced protein levels of p21 (Bedelbaeva et al., 2010). Furthermore, a recent study has suggested that alteration of the cell cycle in injured epithelial cells, especially in proximal tubules, may affect the progression of interstitial fibrosis (Canaud

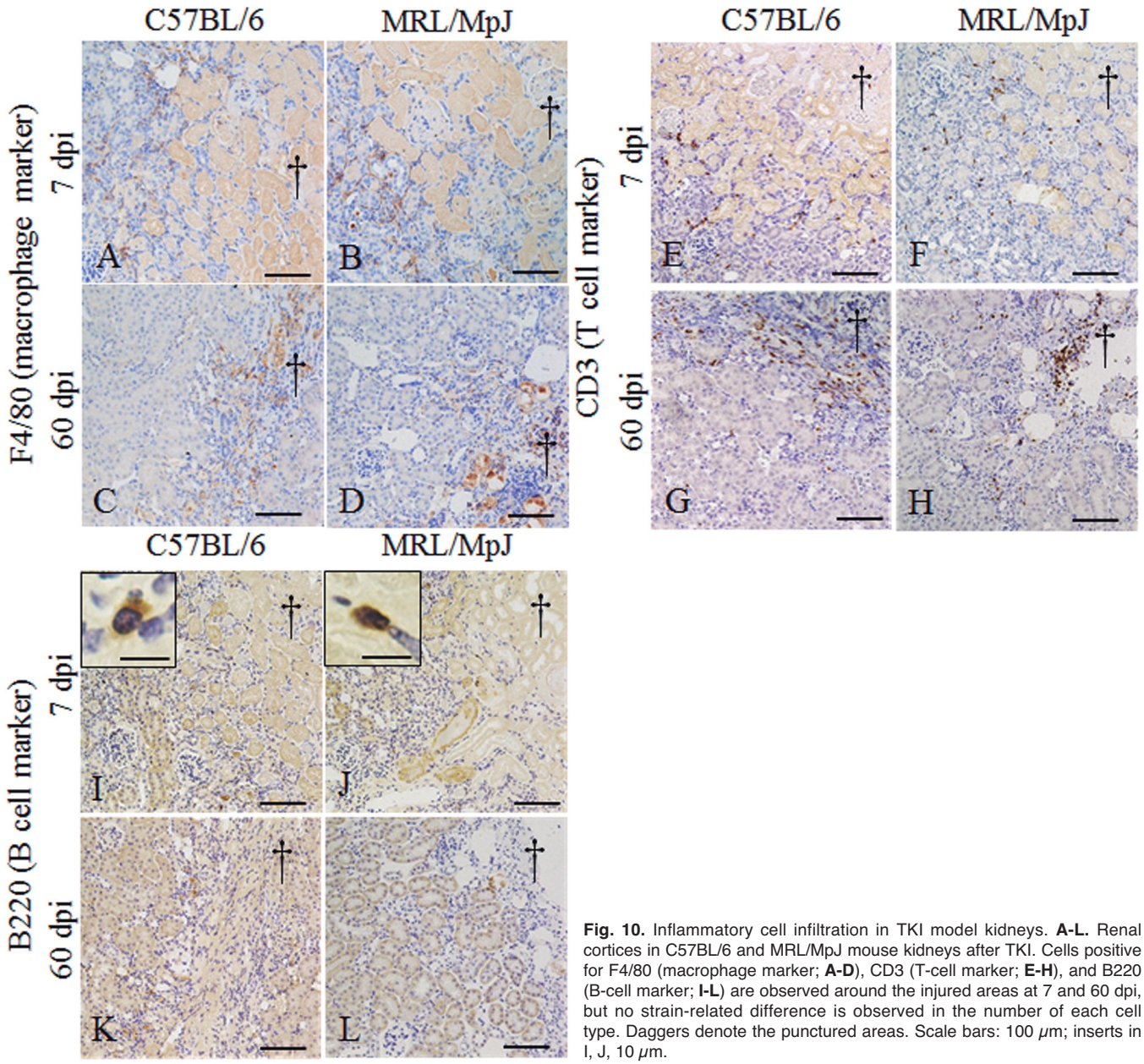

Fig. 10. Inflammatory cell infiltration in TKI model kidneys. **A-L.** Renal cortices in C57BL/6 and MRL/MpJ mouse kidneys after TKI. Cells positive for F4/80 (macrophage marker; **A-D**), CD3 (T-cell marker; **E-H**), and B220 (B-cell marker; **I-L**) are observed around the injured areas at 7 and 60 dpi, but no strain-related difference is observed in the number of each cell type. Daggers denote the punctured areas. Scale bars: 100 μm; inserts in I, J, 10 μm.

and Bonventre, 2015). Therefore, the unique response of tubular epithelial cells to injury caused by genomic factors such as altered cell cycle regulation might contribute to the phenotype of lower fibrotic activity in MRL/MpJ mouse kidneys.

Surprisingly, the kidneys of MRL/MpJ mice showed remarkable calcification, which we considered to be dystrophic calcification, around the injury site after TKI. Dystrophic calcification is usually observed in necrotic tissue and is caused by deviated enzymes, degraded organic phosphorus, and osteogenic proteins (Shimada, 2001). Although renal calcification is frequently observed in the vascular walls of patients with chronic kidney disease (Nguyen et al., 1991), our demonstration of renal calcification in TKI is the first. No clear evidence has explained the pathogenesis of calcification in TKI, but we propose 2 hypotheses to clarify the formation mechanism of calcification observed in MRL/MpJ mouse kidneys: (1) the levels of local or serum ions such as calcium and phosphate differ between C57BL/6 and MRL/MpJ mice, and (2) the presence of calcification-inducible cells in MRL/MpJ mice. Future studies focusing on these hypotheses might help elucidate the kidney repair process, especially the appearance of calcification, in detail.

The collective results of this study demonstrated that injured MRL/MpJ mouse kidneys did not show the wound-healing phenotype reported for the ear, heart, and central nervous system in these mice. However, we found that the renal pathological features after AKI and TKI differed between MRL/MpJ and C57BL/6 mice. In particular, significant differences were observed in the severity of proximal tubule injury in AKI and the formation of tubulointerstitial lesions in TKI. AKI is induced by ischemia and toxins and drugs such as metabolites of ethylene glycols, grapes, raisins, and cisplatin in companion animals (Ross, 2011). Furthermore, TKI inevitably occurs after renal surgery, biopsy, and nephrostomy. The data in this study contribute to the understanding of the pathogenesis and renal repair process in various kidney injuries. Clearly, the genetic background of MRL/MpJ mice is the origin of the unique pathological features observed in this strain after experimental kidney injury. These findings suggest that differences in the kidney repair process may be due to genetic variations between mouse strains, animal species, and human races. Genetic analysis of MRL/MpJ mice, such as quantitative trait loci analysis targeting the phenotypes clarified in this study, are likely to identify the candidate genes crucial for renal repair and may be useful for developing novel therapeutic targets for kidney injury.

Acknowledgements. This study was chosen for the Encouragement Award (undergraduate section) at the 157th Japanese Association of Veterinary Anatomists in Sapporo, Japan (September 9-12, 2014). This study was partially supported by JSPS KAKENHI Grant Numbers 24380156, 24688033, 15H05634, and 15K14873.

References

Alleva D.G., Kaser S.B. and Beller D.I. (1997). Aberrant cytokine expression and autocrine regulation characterize macrophages from young MRL$^{+/+}$ and NZB/W F1 lupus- prone mice. J. Immunol. 159, 5610-5619.

Anders H.J. (2012). Four danger response programs determine glomerular and tubulointerstitial kidney pathology: clotting, inflammation, epithelial and mesenchymal healing. Organogenesis 8, 29-40.

Badid C., Mounier N., Costa A.M. and Desmoullére A. (2000). Role of myofibroblasts during normal tissue repair and excessive scarring: Interest of their assessment in nephropathies. Histol. Histopathol. 15, 269-280.

Bedelbaeva K., Snyder A., Gourevitch D., Clark L., Zhang X.M., Leferovich J., Cheverud J.M., Lieberman P. and Heber-Katz E. (2010). Lack of p21 expression links cell cycle control and appendage regeneration in mice. Proc. Natl. Acad. Sci. USA 13, 5845-5850.

Canaud G. and Bonventre J.V. (2015). Cell cycle arrest and the evolution of chronic kidney disease from acute kidney injury. Nephrol. Dial. Transplant. 30, 575-583.

Cavdar Z., Ozbal S., Celik A., Ergur B.U., Guneli E., Ural C., Camsari T. and Guner G.A. (2013). The effects of alpha-lipoic acid on MMP-2 and MMP-9 activities in a rat renal ischemia and re-perfusion model. Biotech. Histochem. 89, 304-314.

Deb A. and Ubil E. (2014). Cardiac fibroblast in development and wound healing. J. Mol. Cell. Cardiol. 70, 47-55.

Fausto N. (2000). Liver regeneration. J. Hepatol. 32, 19-31.

Foster W., Li Y., Usas A., Somogyi G. and Huard J. (2003). Gamma interferon as an antifibrosis agent in skeletal muscle. J. Orthop. Res. 21, 798-804.

Gourevitch D., Clark L., Chen P., Seitz A., Samulewicz S.J. and Heber-Katz E. (2003). Matrix metalloproteinase activity correlates with blastemal formation in the regenerating MRL mouse ear hole model. Dev. Dyn. 226, 377-387.

Gupta A., Puri V., Sharma R. and Puri S. (2012). Folic acid induces acute renal failure (ARF) by enhancing renal prooxidant state. Exp. Toxicol. Pathol. 64, 225-232.

Hampton D.W., Seitz A., Chen P., Heber-Katz E. and Fawcett J.W. (2004). Altered CNS response to injury in the MRL/MpJ mouse. Neuroscience 127, 821-832.

Ichii O., Otsuka S., Sasaki N., Yabuki A., Ohta H., Takiguchi M., Hashimoto Y., Endoh D. and Kon Y. (2010). Local overexpression of interleukin-1 family, member 6 relates to the development of tubulointerstitial lesions. Lab. Invest. 90, 459-475.

Johnson T.S., Haylor J.L., Thomas G.L., Fisher M. and El Nahas A.M. (2002). Matrix metalloproteinases and their inhibition in experimental renal scarring. Exp. Nephrol. 10, 182-195.

Kamogawa J., Terada M., Mizuki S., Nishihara M., Yamamoto H., Mori S., Abe Y., Morimoto K., Nakatsuru S., Nakamura Y. and Nose M. (2002). Arthritis in MRL/lpr mice is under the control of multiple gene loci with an allelic combination derived from the original inbred strains. Arthritis Rheum. 46, 1067-1074.

Kawano H., Kimura-Kuroda J., Komuta Y., Yoshioka N., Li H.P., Kawamura K., Li Y. and Raisman, G. (2012). Role of the lesion scar in the response to damage and repair of the central nervous system. Cell Tissue Res. 349, 169-180.

Leferovich J.M., Bedelbaeva K., Samulewicz S., Zhang X.M., Zwas D.,

Lankford E.B. and Heber-Katz E. (2001). Heart regeneration in adult MRL mice. Proc. Nat. Acad. Sci. USA 98, 9830-9835.

Lim A.I., Tang S.C., Lai K.N. and Leung J.C. (2013). Kidney injury molecule-1 more than just an injury marker of tubular epithelial cells? J. Cell Physiol. 228, 917-924.

Long D.A., Price K.L., Ioffe E., Gannon C.M., Gnugi L., White K.E., Yancopoulos G.D., Rudge J.S. and Woolf A.S. (2008). Angiopoietin-1 therapy enhances fibrosis and inflammation following folic acid-induced acute renal injury. Kidney Int. 74, 300-309.

Mack M. and Yanagita M. (2015). Origin of myofibroblasts and cellular events triggering fibrosis. Kidney Int. 87, 297-307.

Maeshima A., Yamasguta S. and Nojima Y. (2003). Identification of renal progenitor-like tubular cells that participate in the regeneration process of the kidney. J. Am. Soc. Nephrol. 14, 3138-3146.

Masinde G.L., Li X., Gu W., Davidson H., Mohan S. and Baylink D.J. (2001). Identification of wound healing/regeneration quantitative trait loci (QTL) at multiple time points that explain seventy percent of variance in (MRL/MpJ and SJL/J) mice F2 population. Genome Res. 11, 2027-2033.

Moreno J.A., Izquierdo M.C., Sanchez-Niño M.D., Suárez-Alvarez B., Lopez-Larrea C., Jakubowski A., Blanco J., Ramirez R., Selgas R., Rulz-Ortega M., Egido J., Ortiz A. and Sanz A.B. (2011). The inflammatory cytokines TWEAK and TNFα reduce renal Klotho expression through NFκB. J. Am. Soc. Nephrol. 22, 1315-1325.

Naviaux R.K., Le T.P., Bedelbaeva K., Leferovich J., Gourevitch D., Sachadyn P., Zhang X.M., Clark L. and Heber-Katz E. (2009). Retained features of embryonic metabolism in the adult MRL mouse. Mol. Genet. Metab. 96, 133-144.

Nguyen V.D., Nguyen K.D. and Kamath V. (1991). Unusual feature of soft- tissue calcification in chronic renal failure: tumoral calcification. Comput. Med. Imaging Graph. 15, 397-402.

Qi W., Chen X., Twigg S., Polhill T.S., Gillbert R.E. and Pollock C.A. (2006). Tranilast attenuates connective tissue growth factor-induced extracellular matrix accumulation in renal cells. Kidney Int. 69, 989-995.

Ross L. (2011). Acute kidney injury in dogs and cats. Vet. Clin. North Am. Small. Anim. Pract. 41, 1-14.

Shimada A. (2001). The Japanese Society of Veterinary Pathology General Animal Pathology. 2nd ed. Buneido. Tokyo. pp 50-51. (In Japanese).

Sivakumar S., Palsamy P. and Subramanian S.P. (2010). Impact of D-pinitol on the attenuation of proinflammatory cytokines, hyperglycemia-mediated oxidative stress and protection of kidney tissue ultrastructure in streptozotocin-induced diabetic rats. Chem. Biol. Interact. 188, 237-245.

Sohotnik R., Nativ O., Abbasi A., Awad H., Frajewicki V., Bishara B., Sukhotnik I., Armaly Z., Aronson D., Heyman S.N., Nativ O. and Abassi Z. (2013). Phosphodiesterase-5 inhibition attenuates early renal ischemia-reperfusion-induced acute kidney injury: assessment by quantitative measurement of urinary NGAL and KIM-1. Am. J. Physiol. Renal Physiol. 304, F1099-F1104.

Sugimoto H., Grahovac G., Zeisberg M. and Kalluri, R. (2007). Renal fibrosis and glomerulosclerosis in a new mouse model of diabetic nephropathy and its regression by bone morphogenic protein-7 and advanced glycation end product inhibitors. Diabetes 56, 1825-1833.

Thomas M.E., Blaine C., Dawnay A., Devonald M.A., Ftouh S., Laing C., Latchem S., Lewington A., Milford D.V. and Ostermann M. (2015). The definition of acute kidney injury and its use in practice. Kidney Int. 87, 62-73.

Vallance B.A., Gunawan M.I., Hewlett B., Bercik P., Van Kampen C., Galeazzi F., Sime P.J., Gauldie J. and Collins S.M. (2005). TGF-β1 gene transfer to the mouse colon leads to intestinal fibrosis. Am. J. Physiol. Gastrointest. Liver Physiol. 289, G116-G128.

Yang H.C., Liu S.J. and Fogo A.B. (2014). Kidney regeneration in mammals. Nephron Exp. Nephrol. 126, 50-53.

Accepted September 8, 2015